ARCHITECTURED LAMINATED CERAMICS: BIOINSPIRED TOUGHNENIING STRATEGIES

Yazdani Sarvestani, H[1]*, Backman, D[2], Genest, M[2], and Ashrafi, B[1]*

[1] Aerospace Manufacturing Technology Center, National Research Council Canada, 5145 Decelles Avenue, Montreal, QC H3T 2B2 Canada

[2] Structures and Materials Performance Laboratory, National Research Council Canada, Ottawa, ON K1A 0R6 Canada

* Corresponding author (Hamidreza.Yazdani@nrc-cnrc.gc.ca; Behnam.Ashrafi@nrc-cnrc.gc.ca)

Keywords: *Architectured laminated ceramics; Subtractive manufacturing; Bioinspired design*

ABSTRACT

Ceramics offer many attractive properties including low-density, high compressive strength, remarkable thermal stability, and high oxidation/corrosion resistance. However, these materials suffer from brittleness, which substantially limits the range of their applications, especially when high toughness is required. The exploration of the microstructure of these high performance natural materials has revealed the underlying principles required to achieve a balance between stiffness and toughness. In this study, we present several multilayered ceramic systems with bioinspired architectures with an enhanced toughness and multi hit-tolerance. We have designed stochastic ceramic systems based on the architecture of the American white pelican feather and dragonfly wing. These ceramics were manufactured by stacking laser-engraved/cut architectured ceramic tiles and commercial monomer Surlyn. The mechanics of these multilayered architectured ceramics was investigated both numerically and experimentally by subjecting them to out-of-plane quasi-static and impact loads.

1 INTRODUCTION

Ceramics have been widely used for many decades as structural materials, however due to their inherent brittleness their applications have been primarily limited to compressive loading conditions. General interest in the mechanical behaviour of ceramics is motivated by the in-service demand for structural components which often require the application of brittle materials, because of behaviors such as high stiffness and strength, low density, high temperature stability, oxidation, corrosion, hardness, and wear resistance. Further, most of the current advanced designs in aerospace, marine, automotive and armour industries require high toughness which implies potential limitations for ceramics due to their low fracture toughness [1, 2].

Improving the toughness of ceramics is an advancing challenge. Through the process of evolution, biological materials have optimized their structure-property relationship and produced natural disordered microstructures. Borrowing the design of these biological structures from nature may inspire a promising strategy to overcome inherent brittleness of ceramics. Examples such as bone, bamboo, grassy stem, American white pelican feather, dragonfly wing, or crow skull present different organisms and constituent materials of which their structural properties prevent catastrophic and unexpected failure from fatigue or multi-impacts as shown in Fig. 1. In these biological materials, control of the distribution of material as well as the complex and disordered structural phases generate very stiff, strong, and tough materials. These characteristics are necessary for function, and are traditionally mutually exclusive in traditional engineering materials [2].
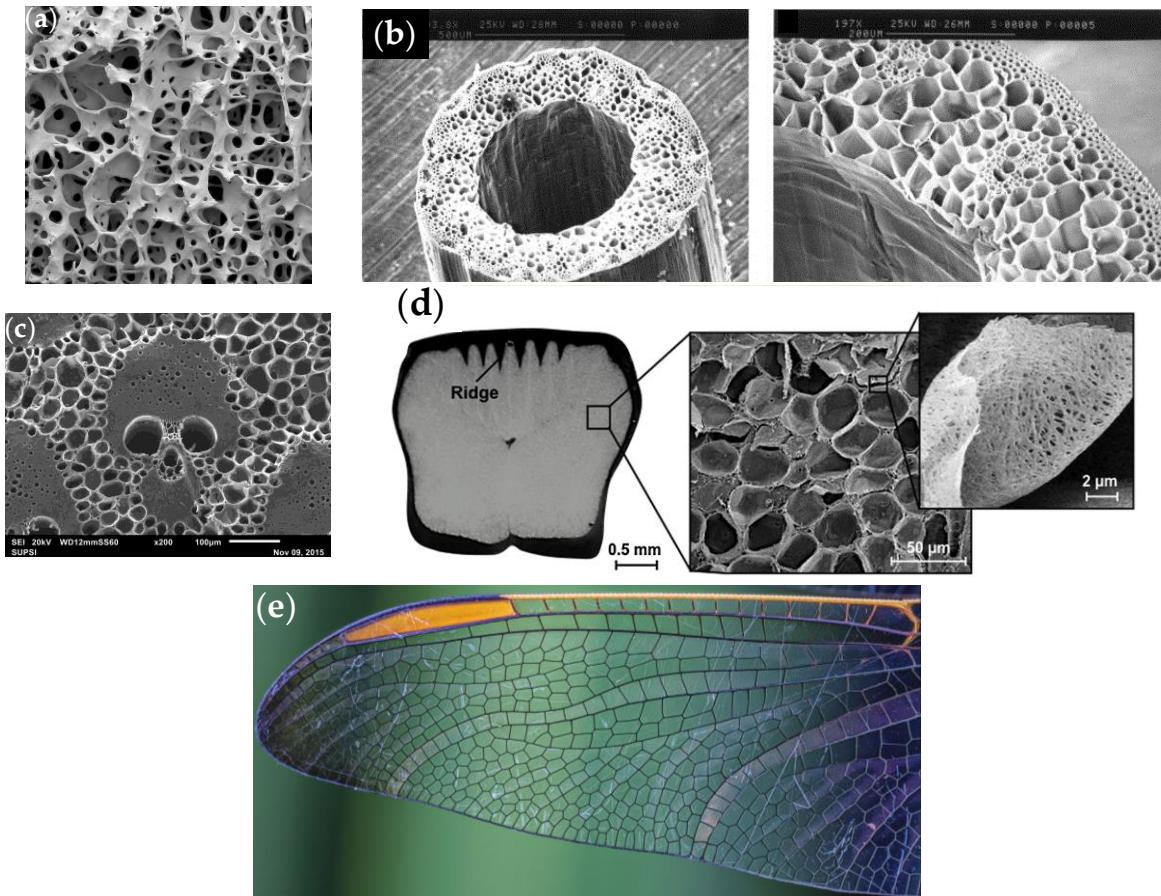
Figure 1. Examples of natural disordered microstructures as a reverse engineering process: (**a**) Bone tissue [3], (**b**) Cross-sectional image of a grass stalk [4], (**c**) Bamboo cell structure [3], (d) Architecture of American white pelican feather [5], and (**e**) Dragonfly wing [5].

Since the early 2000s, due to rapid advances in manufacturing technologies, using the aforementioned design methodologies has become increasingly feasible to accurately produce engineered materials by additive or subtractive manufacturing techniques. Stochastic or disordered designs are another common bioinspired development which through reverse-engineering strategy can improve toughness and multi-impacts behaviors of ceramic materials using advanced manufacturing. Disordered design methodology and its influence on the effective mechanical properties of two- and three-dimensional cellular solids has been the subject of various research efforts [6-12]. However, in these works, special attention was given to lightweight and energy-absorbing applications such as three-dimensional sandwich cores [13, 14]. The arrangement of cell cores is well approximated by a so-called "Voronoi diagram", a crucial tool to measure irregularity. Despite the efforts to duplicate tough materials based on the biological disordered design, only a few successful implementations of these strategies have been reported [6, 15, 16], and less attention has been paid to the design, industrially scalable manufacturing, testing and exploration of toughening and strengthening mechanisms of stochastic ceramic-based bioinspired materials.

We recently demonstrated that laser machining can facilitate manufacturing architectured ceramics with an enhanced resistance to out-of-plane quasi-static and impact loads [17, 18]. By employing these promising bioinspired material architecture principles and disorder-induced mechanisms (quite similar to natural patterns

2

such as bamboo cell structure, and/or dragonfly wing), and by exploiting an industrially scalable, efficient laser material removal system [19], a new class of high material-performance multilayered stochastic ceramic-based bioinspired materials is proposed. A group of multilayered plain, ordered (perfect hexagons) and disordered ceramics was fabricated and tested to show the potential of this strategy in the design of bioinspired stochastic ceramic-based systems. We established toughness, strength, and stiffness maps as functions of laser cut depth and stochasticity to improve the ceramics' mechanical performance in low-velocity, multi-impact loading.

2   Materials and Methods

2.1 Stochastic Design

The models of the stochastic design investigated were constructed by parametric CAD integration. The first step in generating a stochastic design is to define the bounding area, A, in which nucleation points are contained, and the number of desired nuclei, n. The area was chosen as A = 100×100 mm², the same area of the ceramic tiles which used for the manufacturing purpose. A regular hexagonal design, with identical cells having six sides and vertex angles of 120°, can also be considered a stochastic design; for the special case in which all seed points are spaced identically apart as shown in Fig. 2a. This provides an upper bound to the spacing distance of seed points dispersed on a plane. The second step is to calculate the maximum spacing $r_{max} = \sqrt{\frac{2A}{n\sqrt{3}}}$ which accounts for the triangular nature of the distribution (see Fig. 2) [20]. Then, a stochastic design is constructed at any time when a minimum distance between seed points, s, is smaller than the maximum distance rmax. This distance is less than the maximum spacing (i.e., s ≤ rmax). If s is larger, it would be impossible to obtain n number of cells. A new simple parameter is defined so-called "regularity parameter", δ, used in designing the architectured designs and obtained as $\delta = \frac{s}{r_{max}}$. Therefore, it is clear than when δ = 1.0, the hexagonal ceramics condition is met. As the regularity parameter is lowered 0 < δ < 1.0, the seed localizations become distorted and the design transforms stochastically. The degree of stochasticity is inversely proportional to the magnitude of δ. Random points were generated one by one on A. Following each point deposition, its distance relative to all other previously deposited points were measured in a loop. Considering the desired value of regularity parameter δ, if a measured distance during the deposition falls below s, the point is discarded, and a new trial point was loaded. If all distances were greater than s, the new point was kept. This process was repeated up until n number of acceptable points were generated.
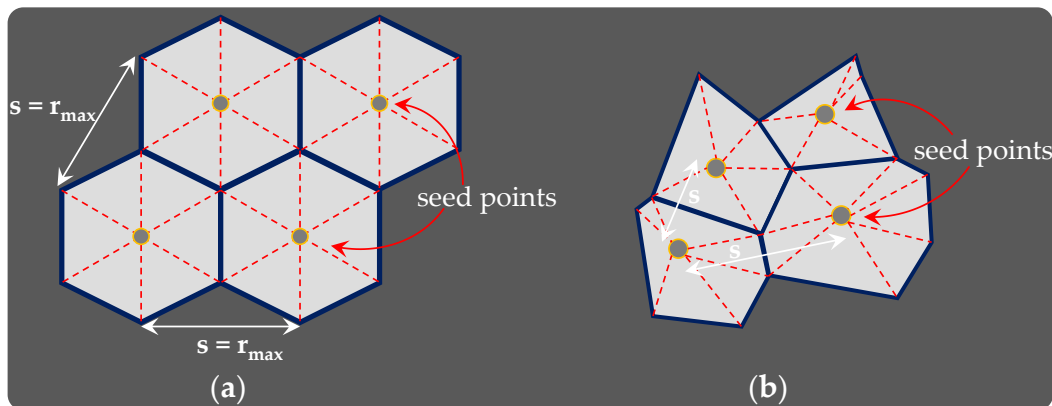

Figure 2. Schematic showing (**a**) Identical spacing between highly ordered seed points, and (**b**) Spacing between disordered seed points.

2.2 Hybrid Manufacturing

A mathematical "regularity parameter" controls the cell stochasticity of the designs for laser ablation. Four degrees of cell regularity, with almost the same number of cells, was chosen for this study which includes an ordered panel of perfect hexagons (δ = 1.0), two pseudo-random panels (δ = 0.8 and 0.5), and a disordered panel (δ = 0.1). In addition, non-architectured samples referred to as "multilayered plain ceramic" or "baseline" were manufactured for comparison. Alumina ceramic tiles of dimension 100×100×0.635 mm3 were purchased off McMaster-Carr and were used to manufacture a three-layer hybrid panel (high-tolerance fired non-porous alumina ceramic with 96% material composition, see Table 1). For each design, three alumina tiles were cut using an Ytterbium picosecond fiber laser (YLPP-25-3-50-R, IPG Photonics, USA). The laser produces a Gaussian spatial profile beam of a maximum power output of 50 W, with a 3 ps pulse duration and a 25 μJ average pulse energy of 1030 nm wavelength. In previous studies [18, 21], a procedure was developed using a circular wobble pattern with the laser scanner to ensure that thermal damage and micro-cracks were minimized. A comprehensive study of the effects of various laser processing parameters was conducted and the optimum process parameter settings that minimized material removal, roughness and manufacturing time were applied [19, 22]. However, due the laser material removal limitations, a stochasticity less than 0.1 was challenging for manufacturing.

Table 1. Material properties of non-porous alumina ceramic tiles.

Property	Value	Property	Value
Tensile strength	220 (MPa)	Modulus of Elasticity	303 (GPa)
Compressive strength	2070 (MPa)	Density	3875 (kg/m^3)

Panels were manufactured to produce two cut depths: (i) 70% and (ii) 100%. The cut depths of 70% was found to have the highest energy absorption performance and multi-hit resistance of different cut depths previously tested [17, 23]. Figure 3 illustrates the high-quality ablated cuts with a damage-free zone where the local high temperature does not change the local material properties. The ordered hexagonal pattern followed an ABA order, where cut designs were offset as shown in Fig. 4. Pattern B was offset such that the vertices of the hexagons were aligned with the centre of the hexagons on pattern A. The disordered panels used three different designs in an ABC order to compose the final manufactured panel. The cut panels were bonded by 101 μm thick Surlyn® interlayers and the deeper cuts are chosen to ensure that the polymer fills in the cavities of the cut ceramic panels during the compression and vacuum curing process. To ensure that the three ceramic tiles were properly aligned, the layered assembly was placed into an aluminum frame and compressed between two tiles. This method allows for uniformity of the final panel thickness across all samples. The ceramic/Surlyn® assembly was then vacuum bagged and set to cure for 5 hours at 146 °C to bond the three ceramic layers into a single panel. The final panel was then demolded from the aluminum frame and sent for impact testing. Consequently, all final manufactured ceramics were 2.10 mm thick which include two 97.5 μm thick interlayers of Surlyn®. It is observed that all full and partial cuts of the panels were filled with Surlyn®.
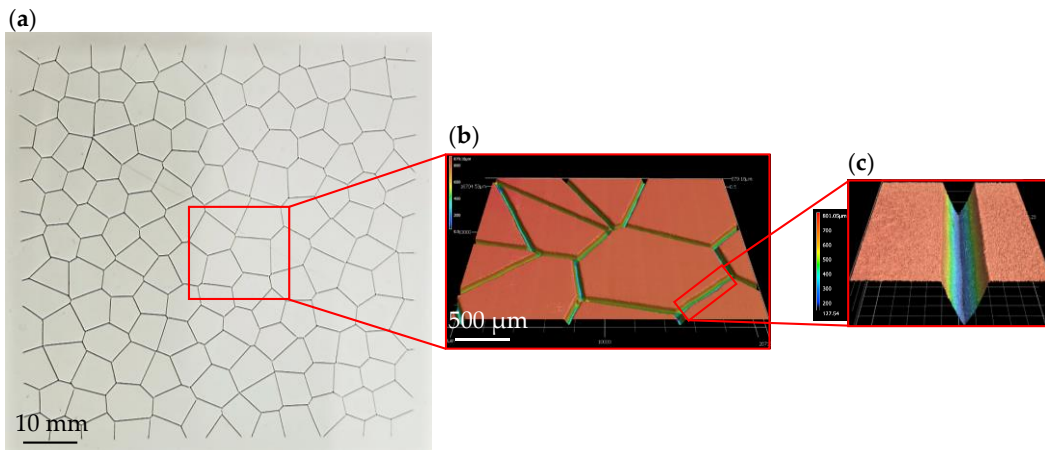
Figure 3. 3D laser scanning microscopy images and topography of (**a**) 70% cut depth and stochastic design, (**b**) Hexagon, and (**c**) Laser machining using picosecond fiber laser (YLPP-25-3-50-R).
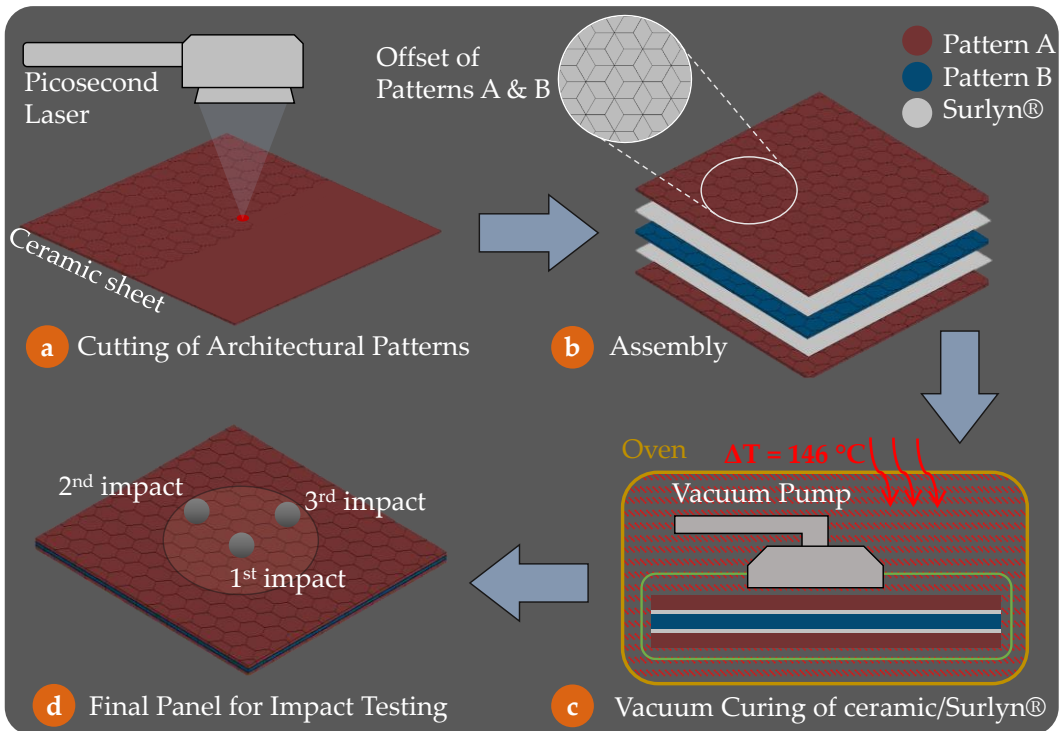

Figure 4. Manufacturing of 3-layer stochastic ceramics highlighting (**a**) Cut patterns with the picosecond laser, (**b**) Assembly schematic with the pattern offset, (**c**) Vacuum bagging and curing of ceramics and commercial monomer Surlyn®, and (**d**) 3 consecutive low-velocity impact test configuration.

2.3 Low-velocity Impact Test Configuration

Three consecutive low-velocity impact tests were performed on the multilayered architectured ceramics using a drop weight machine based on the guidelines given in the ASTM standard D3763 [24]. The impactor had a mass

of 12.5 kg, a diameter of 5 mm with a semi-spherical tip and the impact velocity of 1.36 m/s with the total impact energy of 4.5 J.

3 Experimental Results

The effect of stochasticity on the multi-hit capabilities such as energy absorption performance, stiffness and maximum response load is investigated. Herein, the energy absorption performance is defined as: $\frac{absorbed\ energy}{total\ impact\ energy}$. Figure 5 presents the reaction force-displacement response and displacement and velocity histories of the impactor. The area under the experimental force-displacement curve was measured as the energy absorption of the ceramic systems as shown in Fig. 5a. The area after the maximum load up to the failure point is defined as the crack propagation energy and corresponding mechanisms (see Fig. 5a). The maximum displacement/force, and coefficient of restitution (COR) are also defined in Fig. 5b.
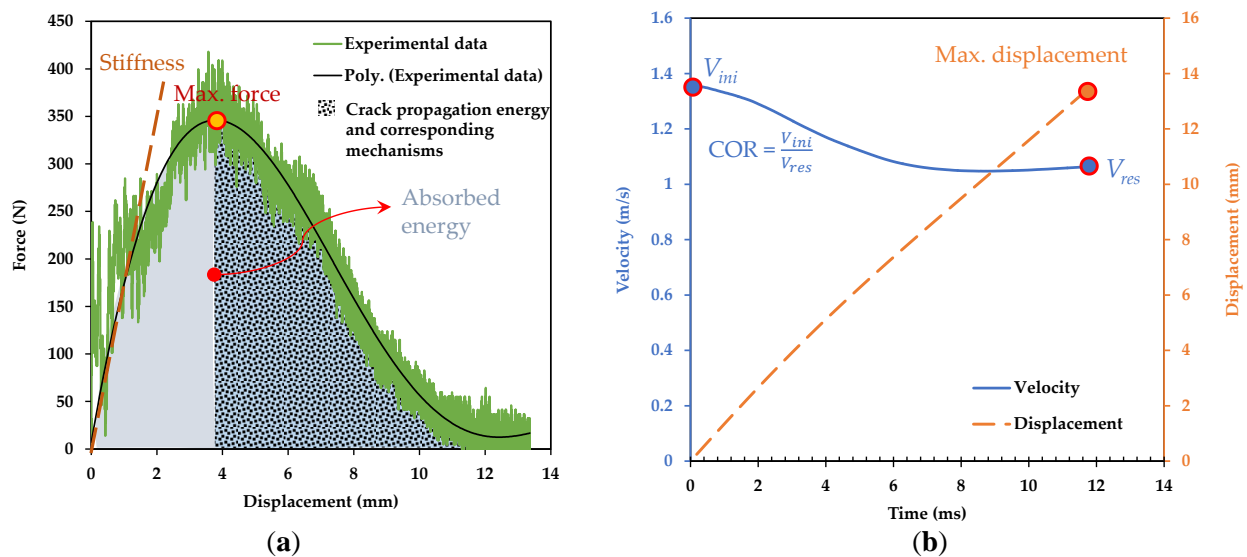

Figure 5. (**a**) Reaction force-displacement response and (**b**) Displacement and velocity histories of the impactor (The maximum displacement/force, energy absorption, crack propagation energy and corresponding mechanisms as well as the coefficient of restitution (COR) are defined).

Figure 6 presents the experimental results for the energy absorption performance, stiffness, and maximum response force of the multilayered architectured ceramics with the stochasticity of δ = 0.1, 0.5, and 0.8, and a perfect hexagonal design (δ = 1.0) as well as the baseline for the 70% and 100% cut-depths. The energy absorption performance of the architectured ceramics impressively increased during the 2nd and 3rd impacts up to 18% and 33%, respectively, unlike the plain ceramic (i.e., baseline). Generally, the 70% cut-depth architectured ceramics have higher energy absorption performance compared to the 100% cut-depth ones for all three impacts up to 55%. Specifically, the 70% cut-depth stochastic ceramic with δ = 0.1 absorbed 10% more energy during the 1st impact and up to 15% and 45% more energy during the 2nd and 3rd impacts compared to the fully-cut stochastic ceramic (100% cut depth with δ = 0.1), respectively. As shown in Fig. 6a, increasing the stochasticity, δ, from 0.8 to 0.1 resulted in an increase in the energy absorption performance of ceramic systems for both partial- and fully-cuts. The crack propagation energy of the ceramic systems is also presented in Fig. 6a. It is seen that the crack propagation energy of the 3-layer architectured ceramics (for δ = 0.1, 0.5, 0.8, and 1.0 with the 70% and 100% cut depths) increased

during the 2nd and 3rd impacts in contrast to the baseline. After the 1st impact, frictional tile sliding becomes more important among all the toughening mechanisms. This mechanism is absent in the baseline. Considering the shear strength of the adhesive interlayer was overcome after the 1st impact, even more energy was dissipated by the plastic deformation of the adhesive interlayers in the architectured ceramic system. Furthermore, the partial-cuts cause the architectured ceramics to dissipate more energy through crack propagation occurred after the maximum response force. The maximum and minimum crack propagation energies occurred the 3rd impact of the 70% cut-depth stochastic ceramic with δ = 0.1 and baseline, respectively. Observing from Fig. 6b, the ceramic's stiffness generally decreases after each impact independent of architecture. The stiffness of the baseline is higher than those of the architectured ceramics (ordered and stochastic designs) for the 1st impact. The reason is that some of the ceramic materials were removed during the laser removal processing and consequently, the architectured ceramic's stiffness was lower when compared to the baseline. However, for the 2nd and 3rd impacts, the perfect hexagonal (δ = 1.0) and stochastic ceramic systems (δ = 0.1, 0.5, and 0.8) have higher stiffness (up to 170%) compared to the baseline. Many cracks were propagated in the plain ceramic following the 1st impact and consequently, the plain ceramic loses its stiffness up to 25% (see Fig. 6b). In addition, the partial-cut ceramics (70% cut depth) have higher stiffness comparted to the fully-cut ceramic (100% cut depth) for all three impacts. As observed from Fig. 6c, the multilayered architectured ceramics have lower response forces compared to the baseline for all three impacts. Among the architectured ceramics, the 70% cut-depth disordered design (δ = 0.1) and 100% cut-depth perfect hexagonal system have the highest and lowest strength, respectively. The strength of the ceramics decreases toward the 3rd impact since some cracks were propagated during the 1st and 2nd impacts. The number of propagated cracks depends on the ceramic system whether it is a partial/fully-cut or a stochastic/ordered design. In summary, the balanced material performance makes the 70% cut-depth stochastic ceramic with δ = 0.1 a competitive candidate with a remarkable multi-hit resistant and stiffness. However, in terms of the strength, the appropriate selection between the 70% and 100% cut depths is dependent on the target application. For example, the 100% cut-depth ceramic has a lower response force compared to the 70% cut-depth one which is a better choice where less response force is required to transfer to the system such as personnel protective equipment.
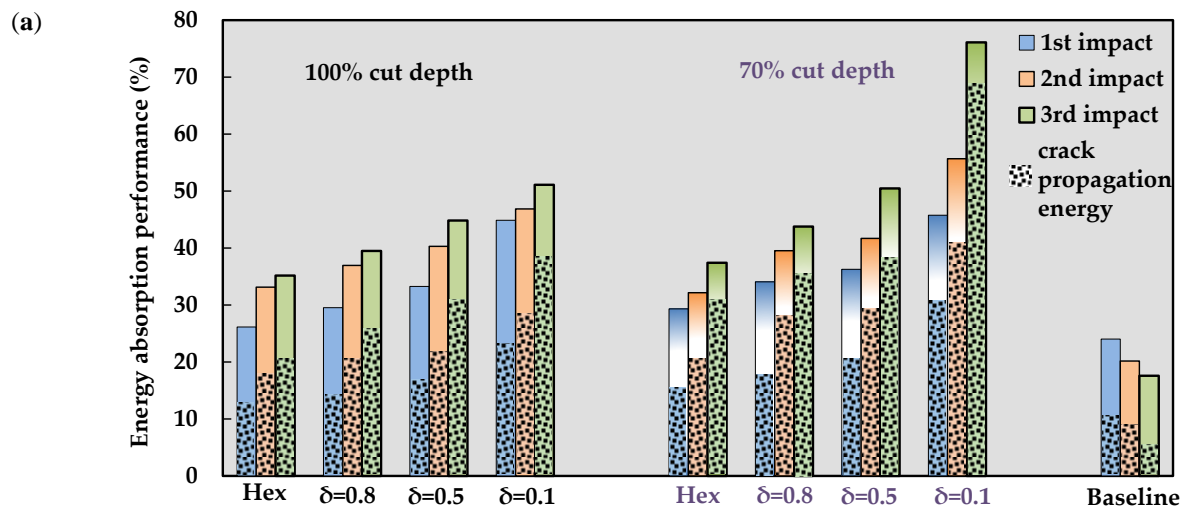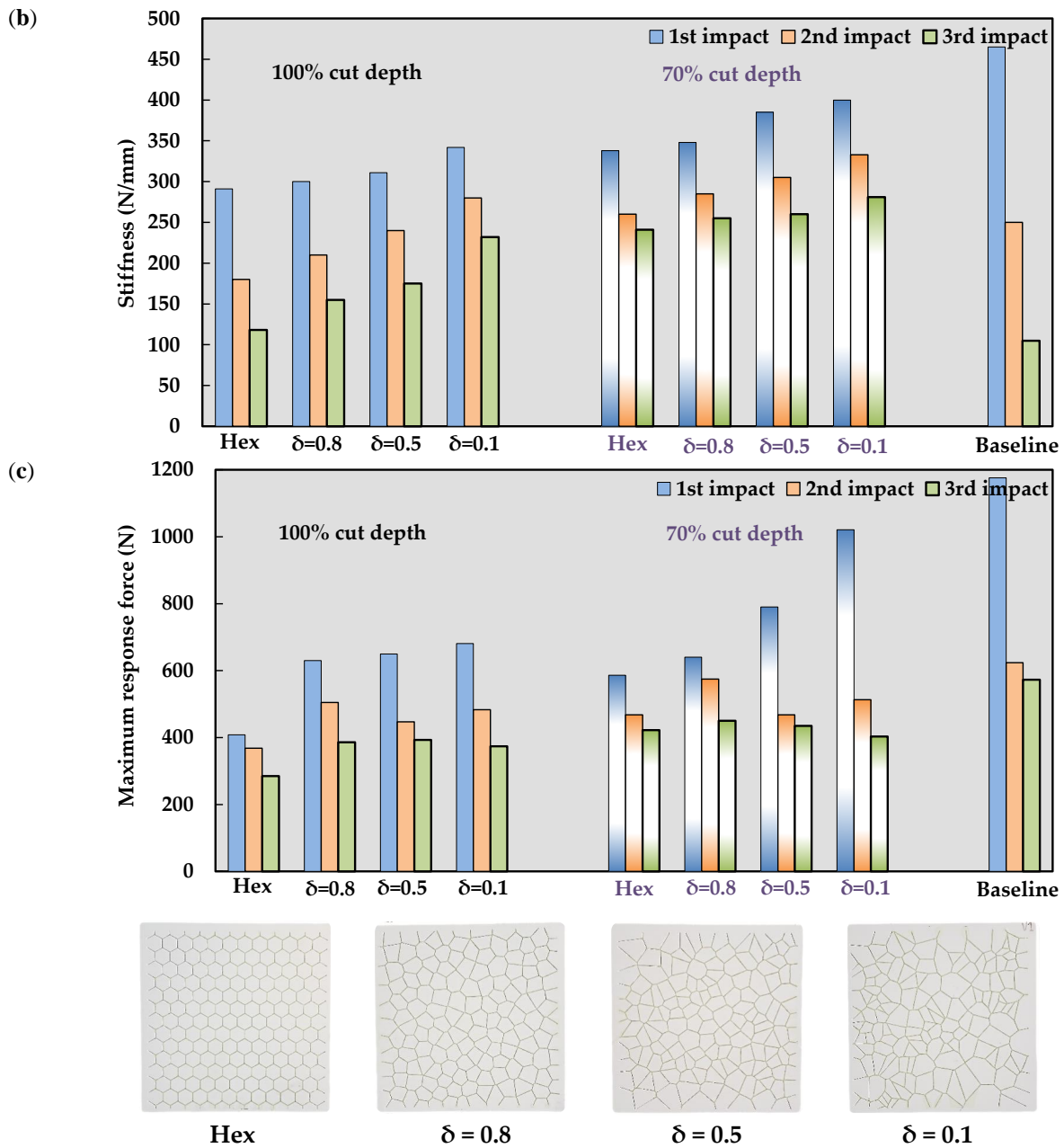
Figure 6. Multi-hit properties of the 3-layer architectured ceramics with the stochasticity of δ = 0.1, 0.5, and 0.8, and a perfect hexagonal design (δ = 1.0) for the 70% and 100% cut-depths as well as the baseline: (**a**) Energy absorption performance, (**b**) Stiffness, and (**c**) Maximum response force.

4   REFERENCES

1.   Kingery, W.D., H.K. Bowen, and D.R. Uhlmann, *Introduction to ceramics*. Vol. 17. 1976: John wiley & sons.

2.   Danzer, R., *A general strength distribution function for brittle materials.* Journal of the European Ceramic Society, 1992. **10**(6): p. 461-472.

3. Gibson, L.J., M.F. Ashby, and B.A. Harley, *Cellular materials in nature and medicine*. 2010: Cambridge University Press.

4. Gibson, L.J., *Biomechanics of cellular solids.* Journal of biomechanics, 2005. **38**(3): p. 377-399.

5. Sullivan, T.N., et al., *Extreme lightweight structures: avian feathers and bones.* Materials Today, 2017. **20**(7): p. 377-391.

6. Wu, K., et al., *Interfacial strength-controlled energy dissipation mechanism and optimization in impact-resistant nacreous structure.* Materials & Design, 2019. **163**: p. 107532.

7. Wang, S., et al., *Crushing behavior and deformation mechanism of additively manufactured Voronoi-based random open-cell polymer foams.* Materials Today Communications, 2020: p. 101406.

8. Chang, B., et al., *Crashworthiness design of graded cellular materials: An asymptotic solution considering loading rate sensitivity.* International Journal of Impact Engineering, 2020: p. 103611.

9. Sun, Y., et al., *Determination of the constitutive relation and critical condition for the shock compression of cellular solids.* Mechanics of Materials, 2016. **99**: p. 26-36.

10. Li, L., et al., *Insight into cell size effects on quasi-static and dynamic compressive properties of 3D foams.* Materials Science and Engineering: A, 2015. **636**: p. 60-69.

11. Huang, Z., et al., *Hidden energy dissipation mechanism in nacre.* Journal of Materials Research, 2014. **29**(14): p. 1573.

12. Huang, Z., et al., *Uncovering high-strain rate protection mechanism in nacre.* Scientific reports, 2011. **1**: p. 148.

13. Li, K., X.-L. Gao, and G. Subhash, *Effects of cell shape and strut cross-sectional area variations on the elastic properties of three-dimensional open-cell foams.* Journal of the Mechanics and Physics of Solids, 2006. **54**(4): p. 783-806.

14. Zhu, H. and A. Windle, *Effects of cell irregularity on the high strain compression of open-cell foams.* Acta Materialia, 2002. **50**(5): p. 1041-1052.

15. Gutiérrez, A., et al., *The role of hierarchical design and morphology in the mechanical response of diatom-inspired structures via simulation.* Biomaterials science, 2018. **6**(1): p. 146-153.

16. Luxner, M.H., et al., *A finite element study on the effects of disorder in cellular structures.* Acta biomaterialia, 2009. **5**(1): p. 381-390.

17. Sarvestani, H.Y., et al., *Multilayered architectured ceramic panels with weak interfaces: energy absorption and multi-hit capabilities.* Materials & Design, 2019. **167**: p. 107627.

18. Sarvestani, H.Y., et al., *Architectured ceramics with tunable toughness and stiffness.* Extreme Mechanics Letters, 2020: p. 100844.

19. Beausoleil, C., et al., *Deep and high precision cutting of alumina ceramics by picosecond laser.* Ceramics International, 2020.

20. Zhu, H., J. Hobdell, and A. Windle, *Effects of cell irregularity on the elastic properties of 2D Voronoi honeycombs.* Journal of the Mechanics and Physics of Solids, 2001. **49**(4): p. 857-870.

21. Rahimizadeh, A., et al., *Engineering toughening mechanisms in architectured ceramic-based bioinspired materials.* Materials & Design. **198**: p. 109375.

22. Esmail, I., et al., *Engineered net shaping of alumina ceramics using picosecond laser.* Optics & Laser Technology, 2021. **135**: p. 106669.

23. Sarvestani, H.Y., et al., *Architectured ceramics with tunable toughness and stiffness.* Extreme Mechanics Letters, 2020. **39**: p. 100844.

24. Fragassa, C. and G. Minak. *Standard characterization for mechanical properties of photopolymer resins for rapid prototyping*. in *1st Symposium on Multidisciplinary Studies of Design in Mechanical Engineering, Bertinoro, Italy (Jun. 25-28, 2008)*. 2008.